

Flexure-shear behavior of precast concrete deck panels with cast-in-place concrete topping

Robert K. Dowell and Roy Auer

The Garden Grove Boulevard Undercrossing (East) widening in Orange County, Calif., (recipient of PCI's 2007 Design Award for Best Rehabilitated Bridge) was initially designed as a prestressed concrete box-girder superstructure (**Fig. 1**). However, it was altered to use precast concrete girders and permanent precast, prestressed concrete deck slabs with a cast-in-place concrete topping slab. The modified design had several purposes:

- to maintain vertical clearance during construction (because falsework was no longer required)
- to minimize the construction schedule
- to reduce costs

Precast concrete deck-panel tests demonstrated that the precast concrete deck slabs and the cast-in-place concrete topping act compositely through large displacements, allowing their use on the Garden Grove widening as well as many other bridges along this corridor on the design-build project. **Figure 2** shows typical precast concrete slabs at the casting yard and positioned between girders before placement of the cast-in-place concrete topping slab that completed the section and made the final riding surface.

To alleviate any concerns regarding composite behavior between the roughened precast concrete slab and the cast-

Editor's quick points

- Full-scale precast concrete deck slabs designed for bridge structures were tested to failure under simple bending with varying levels of roughness between the precast concrete slab and cast-in-place concrete topping slab.
- The measured and observed shear failures for all three composite slabs tested in positive bending are compared to analytically determine force and displacement values at failure.
- Theoretical and measured crack widths and plastic hinge rotations at midspan are also compared in the paper.

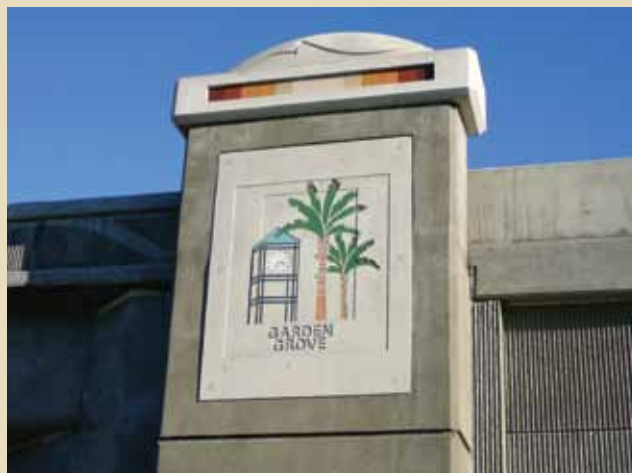


Figure 1. The Garden Grove Boulevard undercrossing (east) widening in Orange County, Calif.

in-place concrete topping slab, which has no reinforcement crossing between slabs, structural tests were performed. The precast concrete deck slabs were cast at a precast concrete plant and shipped to the bridge site where the cast-in-place concrete topping slab was placed and cured. The composite slabs were then shipped for structural testing.

Five full-scale structural tests and prediction analyses were conducted to large displacement and failure to demonstrate that precast concrete deck panels with a cast-in-place concrete topping slab act compositely in linear bending.¹⁻³ The structural tests included the precast concrete deck panel acting alone, the composite slab (precast and cast-in-place concrete) loaded in negative bending (upside down), and three tests of the composite slabs loaded in positive bending.

Only the three composite, positive bending structural tests are considered in this paper because the other two tests do not represent expected loading conditions. All of the tests were conducted in simple bending with full-width supports at the ends of the precast concrete slab and full-width loading at the center of the span (**Fig. 3**).

Prediction analyses by Dowell and Smith¹ included only the flexural force-deformation response of the slabs to failure without considering the final failure mode at large displacement. However, the full-scale structural tests showed that failure of all three deck slabs occurred in shear along a single inclined flexure-shear crack plane. This paper explores the measured test results approaching and at the onset of shear failure and compares them with



Slabs at precast concrete plant



Slabs at bridge site

Figure 2. Precast concrete slabs at precast concrete plant and in place between girders at bridge site.



Figure 3. Tests were conducted in simple bending with full-width supports at ends of precast concrete slab and full-width loading at center span.

results determined from a unique application of the modified compression field theory.⁴ Measured displacements at failure were far larger than expected from service loading and from severe seismic shaking.

In contrast to the traditional application of this theory, the degrading shear force capacity was found as a function of midspan vertical displacement (**Fig. 4**). The vertical displacement was related by geometry to the number of cracks, crack spacing, and crack widths through the midspan region.

A deck panel of a bridge in the field loaded by gravity forces of dead and live loads will fail once the applied loads exceed the peak force capacity, which is found from the force-deformation characteristics of the composite deck. Any additional load beyond the force capacity cannot

be statically equilibrated by the deck and is realized as an inertial force with dynamic response of mass multiplied by downward acceleration. Hence, in the field, the softening branch of the force-deformation response, beyond peak force, is not a possible equilibrium position.

In the laboratory, however, the complete force-deformation response of the deck to failure can be found by applying the load in displacement control rather than in force control. In this approach the displacement is increased at midspan and the force at that displacement is measured, allowing the complete behavior to be determined, including the post-peak, or softening, branch of the response.

Onset of failure in the field occurs at peak force and associated displacement. Similarly, if the loads were applied in force control in the laboratory, simulating gravity loads in the field, the structure and test setup would become unstable at peak force and measured results at larger displacements could not be obtained.

Based on the overall geometry of the plastically displaced structure (displaced structure profile minus the elastic displacements), as well as the number and spacing of cracks, the average crack width in the critical region across the midspan can be related to the centerline vertical displacement. Modified compression field theory directly relates crack width to the concrete shear capacity from aggregate interlock. As the cracks widen from increased flexural displacements, the shear capacity drops considerably. Because the deck slabs contain no shear reinforcement, the concrete resists all of the shear force and provides all of the shear capacity, which degrades with increased vertical displacement and widening of cracks.

Shear force demand near midspan is equal to half of the applied force. Hence, the applied force is always twice the

shear force at the critical section. If this force decreases with increased displacement, the applied force must also decrease. After the onset of shear failure (defined as the intersection of the force-deformation and shear capacity curves [Fig. 4]), the applied force decreases with increased displacement, following the descending shear force capacity curve as crack widths and midspan displacements increase.

The shear force capacity versus vertical displacement curve is plotted on the same graph as the predicted force-deformation curve¹ that considers only flexure. Where these two curves intersect represents expected shear failure. Before the onset of shear failure, the response follows the flexural behavior.

At displacements beyond this point, the response follows the declining shear failure curve. Thus, over the complete range of displacements the deck force-deformation behavior initially follows the flexural curve to large displacements and abruptly changes direction when this curve intersects the shear capacity curve. The force-deformation response then follows the declining shear capacity curve.

This paper presents an approach for determining the shear capacity of precast, prestressed concrete deck panels with a cast-in-place concrete topping slab. Analytical results are compared with measured and observed shear failures of the three nominally identical, full-scale deck panels tested in the laboratory. Crack widths in the critical regions were measured throughout the tests and provide important information regarding the onset of shear failure and concentration of failure along a single inclined crack plane. The single flexure-shear crack that ultimately resulted in shear failure was measured throughout all three tests (labeled tests A, B, and C).

Measured and analytical results

Figure 4 shows the predicted and measured force-deformation curves for the three deck slabs. The shear force capacity-deformation curve is also plotted, clearly showing excess shear capacity at small displacements and a rapid decline in shear capacity with increased vertical displacement. A single force-deformation prediction curve is given for the three test units because they were nominally the same. The test variable was the applied roughness on top of the precast concrete slabs with coarse-broom, medium-broom, and carpet-drag finishes. Because no longitudinal slip was observed or measured at the precast-cast-in-place concrete slab interface, this difference of roughness between test units had no effect on their responses or failure modes.

At about 0.7 in. (18 mm) of relative vertical displacement (subtracting bearing-pad deformations at the end reaction points), the decreasing shear force capacity curve intersects measured and predicted force-deformation curves (Fig.

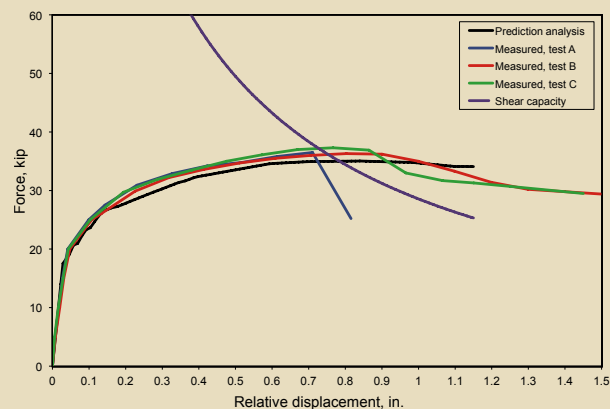


Figure 4. Measured and predicted force-deformation responses with shear capacity for all three decks. The shear force capacity–deformation curve shows excess shear capacity at small displacements and a rapid decline in shear capacity with increased vertical displacement. Note: 1 in. = 25.4 mm; 1 kip = 4.448 kN.

4). Intersection of the shear force capacity curve with the predicted force-deformation flexural response represents the failure point from analysis. The predicted force-deformation response in Fig. 4 was calculated before the tests were conducted, but the shear force capacity curve was determined after the tests (post-test analysis) as part of the current research into shear failure. Thus, the shear force capacity curve is not a prediction.

Together these two curves represent the complete force-deformation response determined from analyses, including the initial flexural behavior to large displacements, the onset of shear failure at the intersection of curves, and softening post-shear failure behavior. Because the applied force was twice the shear force at the critical section, force values of the shear force capacity curve plotted in Fig. 4 were doubled to allow plotting on the same graph as the force-deformation curves.

The three composite decks tested in positive bending were nominally the same. Therefore, it would be expected that the force-deformation responses and failure modes would also be the same. Figure 4 shows that the flexural responses are similar, but onset of shear failure occurs at different displacements and force degradation develops at different rates (slopes). However, the analytical results match the average test results well. Scatter in the measured results, for nominally identical slabs, indicates the limit to how close analytical results can get to the measured behavior of any single slab.

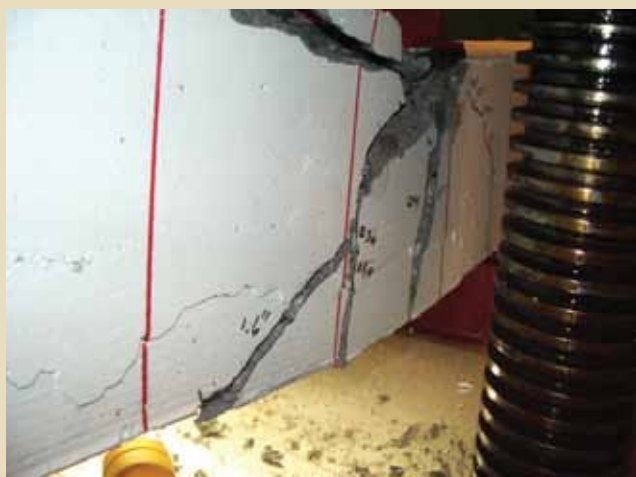
At the intersection of the shear force capacity and force-deformation curves, the negative slope of the shear capacity curve decreased in magnitude and was not so severe. The relative slope between the curves was small. Thus, a slight shift in the shear force capacity near the intersection point can result in a large horizontal shift of the intersection between curves and expected failure displacements. Because the displacement was relatively large at failure



Deck A



Deck B



Deck C

Figure 5. Shear failure of the three decks.

and had a small force-deformation slope (or tangent stiffness), there was little change in force by shifting the intersection point left or right for these three slabs.

The post-test force-deformation analysis followed the declining shear force capacity curve at displacements that are beyond the intersection point, whereas the original

prediction analysis¹ did not consider shear failure.

At the time of the structural tests, it was observed that the deck slabs failed in shear along a single, wide-open, inclined flexure-shear crack (**Fig. 5**). It was not obvious at the time of observation that the gradual force reduction, with increasing displacement, for tests B and C—starting at about 0.9 in. (23 mm) of relative displacement—was associated with the onset of shear failure. For test A, **Fig. 4** shows that shear failure occurred at about 0.7 in. (18 mm) of relative displacement (0.6 in. [15 mm] of plastic displacement) due to sudden concentration and opening of the critical crack (**Fig. 6** shows measured crack widths), as the large negative slope of the force-deformation curve from this test indicates (**Fig. 4**).

Figure 6 shows measured and theoretical crack widths for the three decks tested. In the analysis approach the average crack width was determined as a function of the applied vertical displacement at midspan, with the assumption that the crack widths through the critical region would be approximately constant (this can be justified based on the tension-shift effect). The measured results in **Fig. 6** demonstrate that this assumption was reasonable before the onset of shear failure.

Once shear failure started at displacements beyond peak force, the crack at a single critical location opened more than the other cracks, which tended to close or reduce in width. This critical location represents instability and localization of the response, and the final separation of the member occurred along this inclined failure plane. Theoretical and measured crack widths at the onset of shear failure were approximately the same for the three deck panels at the critical crack location.

Figure 7 compares the midspan theoretical plastic rotations based on applied vertical displacements and rigid-body geometry considerations with plastic rotations determined from summing the measured crack widths in **Fig. 6**. The similar results for all three decks demonstrate that all significant crack widths were measured accurately, as the measured plastic rotations were found by summing individual plastic rotations attributed to each considered crack.

Theoretical plastic rotations were found based on the rigid-body geometry of a simple beam with a concentrated plastic hinge at midspan. Similarly, based on this rigid-body model, vertical plastic displacements at midspan were determined from plastic rotations that were calculated from the measured crack widths. Midspan displacements derived from the measured crack widths compared well with the applied vertical displacements (**Fig. 8**). Overall, the results were similar, showing that most of the plastic displacements came from three or four primary cracks, depending on the slab.

Figure 5 provides photos of final inclined shear failures for

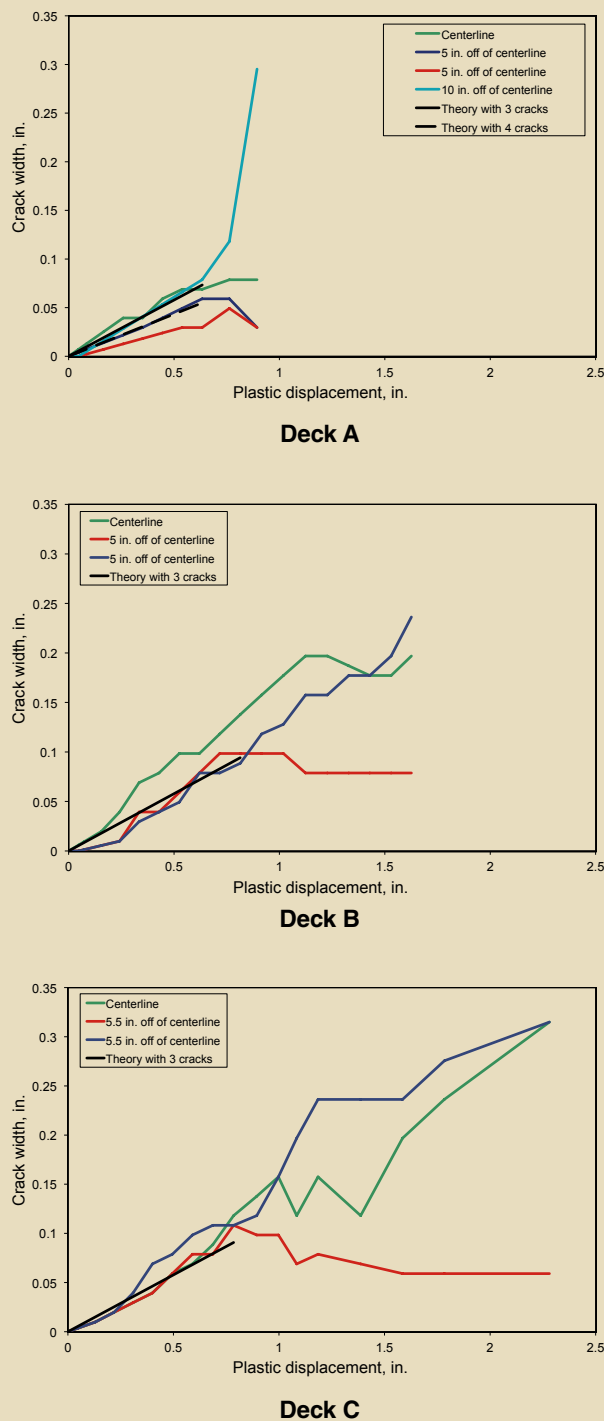
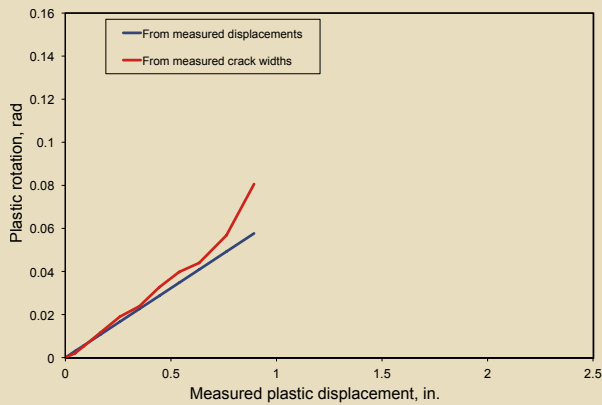
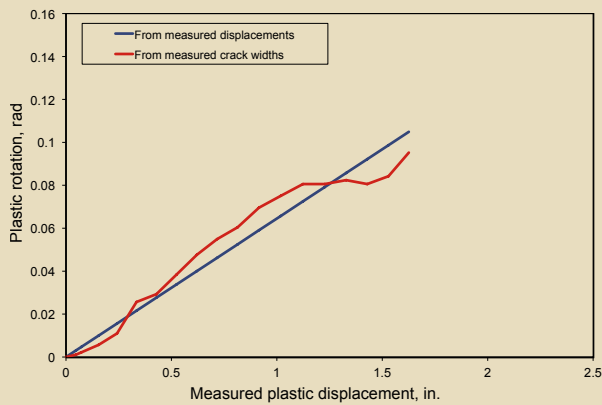


Figure 6. Measured and theoretical crack widths for each of the three decks. Note: 1 in. = 25.4 mm.

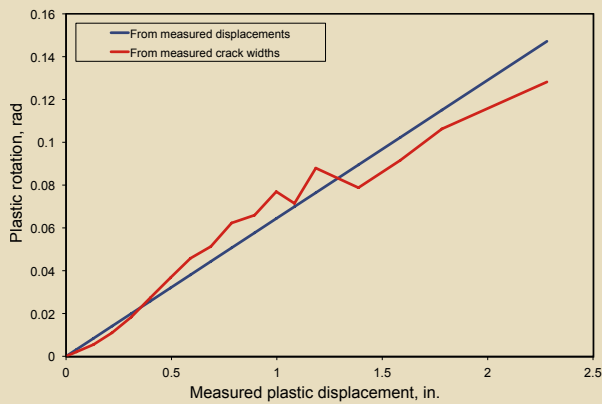
each deck slab. The composite slabs were painted white with vertical red lines drawn at 6 in. (150 mm) spacing. At this stage, the tests were complete and the slab had separated into two pieces. **Figure 9** shows the primary cracks sketched in elevation view, and **Fig. 10** shows these cracks idealized for purposes of determining plastic hinge rotations and plastic displacements from measured crack widths. There were three primary cracks that formed for decks B and C and four primary cracks for deck A.



Deck A



Deck B



Deck C

Figure 7. Measured and theoretical plastic rotations for each of the three decks. Note: 1 in. = 25.4 mm.

Figures 11 and 12 show idealized opening of the cracks, plastic rotation, and final shear failure with separation of the slabs into two pieces. For all three decks, the final shear failure plane started as a flexure crack at the extreme tension fiber some distance from midspan, became a flexure-shear crack as the loading increased, and finally broke off the corner of the slab (at the junction between initial flexure crack and inclined flexure-shear crack) as one side of the structure completely separated and moved down rela-

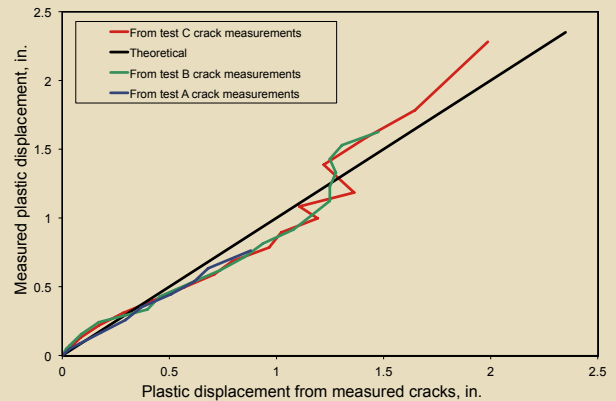


Figure 8. Measured and theoretical plastic displacements for all three decks. Note: 1 in. = 25.4 mm.

tive to the other side (Fig. 5). These were full-width cracks and failure planes. The corner that broke off in elevation view also occurred across the full width of the slab.

Deck A failed at the flexure-shear crack that initiated in flexure 10 in. (250 mm) from midspan (the fourth crack to form and second crack from midspan). Decks B and C, however, failed at flexure-shear cracks that initiated in flexure 5 in. (130 mm) from midspan. None of the structures failed at the midspan crack because of reduced shear, though this was the first crack to form in all cases because it has the largest moment. The midspan crack tended to stay vertical and remained a flexure crack because the shear force through this region was essentially zero as the shear force diagram transitioned from positive to negative shear across the width of the loading head.

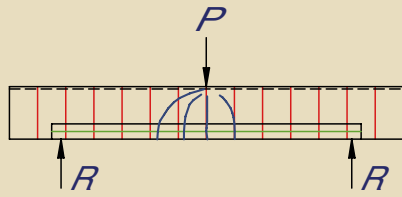
Determining shear force capacity

With the average crack width known from rigid-body geometry of the deformed test slab, the concrete shear capacity can be determined directly from modified compression field theory. Necessary equations were developed to relate the vertical displacement at midspan, plastic rotation at the critical section, and average crack width through the critical region.

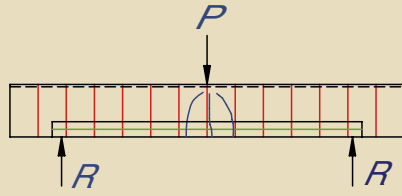
The rotation at the end of the span θ_{pe} , attributed to plastic hinging at midspan, is calculated as a function of the midspan plastic displacement Δ_p and span length between supports l .

$$\theta_{pe} = \frac{\Delta_p}{\left(\frac{l}{2}\right)} = 2 \frac{\Delta_p}{l}$$

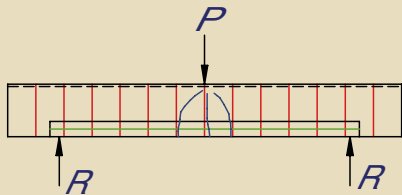
The total plastic rotation θ_p at the critical section is twice the rotation at the end of the span (Fig. 12).



Deck A



Deck B



Deck C

Figure 9. Elevation-view sketches illustrating the observed primary crack patterns for the three composite decks. Note: P = load; R = reaction force.

$$\theta_p = 4 \frac{\Delta_p}{l}$$

The amount of plastic rotation θ_{cr} attributed to a single crack is found from the crack width w at the centroid of prestressing steel divided by the distance between tension and compression centroids jd , found from the difference between d and $a/2$.

$$\theta_c = \frac{w}{\left(d - \frac{a}{2}\right)} = \frac{w}{jd}$$

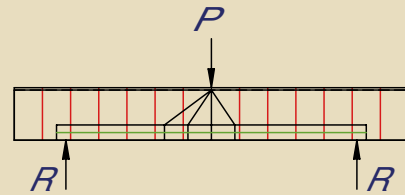
where

j = a constant

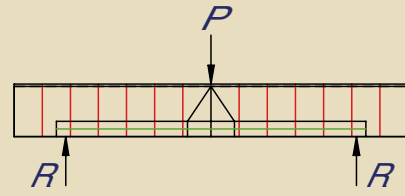
d = distance from the extreme compression fiber to centroid of primary tension reinforcement

a = depth of compression block

Approximately the same moment develops through the



Deck A



Decks B and C

Figure 10. Idealized primary crack patterns for the three composite decks were sketched in elevation to determine plastic hinge rotations and plastic displacements from measured crack widths. Note: P = load; R = reaction force.

region of critical cracking due to a tension-shift effect, allowing strains and crack widths to be taken as constant through the plastic hinge region (Fig. 11 and 12). Thus, the total plastic rotation of the critical section can also be found as the summation of all tributary crack rotations.

$$\theta_p = n\theta_{cr} = n \frac{w}{\left(d - \frac{a}{2}\right)} = n \frac{w}{jd}$$

where

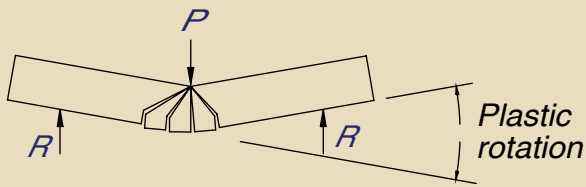
n = number of primary cracks

By equating this definition of plastic rotation, based on average crack width w and number of cracks n , to the plastic rotation expression that is a function of plastic displacement Δ_p and span length l , the average crack width w can be found as a function of the plastic displacement Δ_p at midspan.

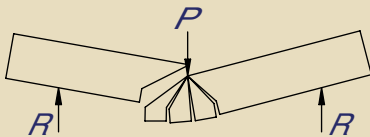
$$4 \frac{\Delta_p}{l} = n \frac{w}{jd}$$

This equation can be rearranged to solve for the average crack width w .

$$w = 4 \frac{\Delta_p}{nl} jd$$

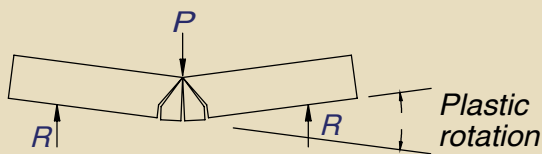


Primary flexure-shear cracks before onset of shear failure

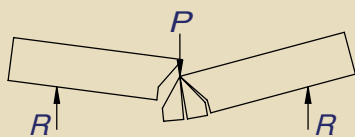


Concentration of shear failure along single inclined shear crack

Figure 11. Idealized crack opening and plastic rotation at midspan and final shear failure for deck A. Note: P = load; R = reaction force.



Primary flexure-shear cracks before onset of shear failure



Concentration of shear failure along single inclined shear crack

Figure 12. Idealized crack opening and plastic rotation at midspan and final shear failure for decks B and C. Note: P = load; R = reaction force.

The crack width calculated in the previous equation is taken at the centroid of the prestressing steel. In the modified compression field theory it is assumed that crack widths and longitudinal strains are constant through the depth of the member. To allow for linear variation of these quantities over the member depth due to bending, the authors of the modified compression field theory suggest using the strains and crack widths at a given distance from the cen-

teroid which depends on the presence or absence of shear reinforcement. The presence of shear reinforcement affects the section's ability to redistribute shear stresses.

Crack spacing s is equal to three times the distance from the centroid of the reinforcement to the extreme tension fiber of the concrete section c .

$$s = 3c = 3(3.25/2) = 4.9 \text{ in. } \therefore s \approx 5 \text{ in. (130 mm)}$$

This crack spacing of 5 in. (130 mm) agrees well with the average measured crack spacing of 5 in. from tests on decks A and B and 5.5 in. (140 mm) from deck C. Thus, constant crack spacing s of 5 in. is used for all analyses presented in this paper.

Cracks initially formed in flexure, extending vertically from the extreme tension face of the concrete. As the load and displacement increased, the cracks extended up the section height. The first crack that formed was at the maximum moment location, directly under the applied load at midspan. This crack continued to widen and extend vertically with increasing displacement. At some point in the loading sequence, two additional flexural cracks formed, one on either side of the first crack. These two cracks were subjected to significant shear, and after widening and extending vertically they started to rotate toward the point of load application, becoming flexure-shear cracks.

Crack patterns followed the trajectories of the principal compressive stresses, which are traditionally represented as compressive struts in a strut-and-tie model for reinforced concrete members that have shear reinforcement. However, in this idealization, the shear reinforcement is assumed to take the vertical component of the compression strut, while the primary reinforcement balances the longitudinal strut component.

The slabs discussed in this paper had primary longitudinal reinforcement but no vertical shear reinforcement. Therefore, they could not equilibrate the compression strut forces from the concrete based on a strut-and-tie analysis. Slabs with no shear reinforcement must balance the shear forces directly through the concrete, which is challenging when wide flexure and flexure-shear cracks develop with large vertical displacements.

As the flexure-shear cracks widened with increased vertical deflection of the member, their ability to transfer shear stresses across the crack reduced to the point that global failure occurred from shear slip along one of the flexure-shear cracks. The modified compression field theory directly recognizes this loss of shear strength with an expression for concrete shear stress capacity v_{ci} as a function of crack width w and maximum aggregate size q .



Table 1. Measured displacements at onset of shear failure

Test panel	Target displacement, in.	Total measured displacement, in.	Relative displacement, in.	Plastic displacement, in.
A	0.8	0.800	0.710	0.634
B	1.0	1.00	0.900	0.814
C	1.0	1.00	0.865	0.785

Note: 1 in. = 25.4 mm.

$$v_{ci} = \frac{2.16\sqrt{f'_c}}{0.3 + \frac{24w}{q + 0.63}}$$

where

f'_c = specified compressive strength of concrete

This expression provides the shear stress capacity at a crack along the orientation of the crack. It demonstrates the ability of the open crack to transfer shear via aggregate interlock and indicates the reduction in this capacity with increased crack width.

The previous expression was originally derived for members in pure shear, with parallel crack walls. Thus, the shear force capacity of the section is found by multiplying the shear stress capacity by the effective section area along the crack plane and then finding the vertical component of this force. The shear force capacity V_{ci} oriented along the crack plane at angle θ from the horizontal can be calculated.

$$V_{ci} = v_{ci}(bk) = v_{ci}\left(b\frac{jd}{\sin\theta}\right)$$

where

b = slab width

k = crack length along incline

The vertical shear force capacity V_c is the vertical component of the previous expression.

$$V_c = V_{ci}\sin\theta = v_{ci}\left(b\frac{jd}{\sin\theta}\right)\sin\theta = v_{ci}(bjd)$$

For a section in bending, however, the crack width varies with distance from the centroid and a reasonable average crack width is recommended⁴ to obtain an average shear stress capacity for the inclined section, providing a simple approach to determine the shear force capacity of

the member. For members with shear reinforcement, the crack width at the neutral axis of the section is chosen as w , whereas for members with no shear reinforcement, the maximum crack width at the extreme tension fiber is suggested⁴ as a reasonable approximation for w .

The maximum crack width at the concrete tension surface is used for design purposes because it is somewhat conservative, comparable to results from a dual section analysis.⁴ Such an approach is reasonable for design, allowing an added factor of safety against shear failure, but not for understanding how a structure failed in the laboratory where the actual force at failure and the failure mechanism need to be understood. Here the critical average crack width is taken as 0.75 of the moment arm jd , which is 0.75 of the maximum crack width at the extreme tension fiber. This splits the difference between using 0.5 for members that have shear reinforcement and the conservative approach of using 1.0 for members without shear reinforcement.

Test results show that deck A formed four primary full-width cracks: one at midspan, two spaced 5 in. (130 mm) on either side of the midspan crack, and a fourth crack 10 in. (250 mm) from the midspan crack. This fourth crack started as a flexure crack that became a flexure-shear crack and, ultimately, the final failure plane for the test specimen. Decks B and C formed only three primary cracks, with the center flexural crack widening and extending as displacements increased. The two additional cracks, at about 5 in. on either side of midspan, started as flexural cracks and became flexure-shear cracks as the loading and displacements increased. One of these flexure-shear cracks formed the final failure plane for the specimens. The flexural cracks remained vertical at midspan because of the lack of shear effects at this location.

Discussion of results

As mentioned previously, the tests were conducted in displacement control. **Table 1** lists the target displacements, total measured displacements, relative displacements, and plastic displacements at midspan at the onset of shear failure. Relative displacements represent total deformations of the member because they are the measured displacements minus the measured deformations of the bearing pads at the end supports. This relative displacement was used for

plotting the various force-deformation curves in Fig. 4. Results from analysis were also given in terms of relative displacement because the end supports were modeled with rigid vertical reactions.

Shear failure occurred between 0.7 in. and 0.9 in. (18 mm and 23 mm) of relative displacement for the three decks (Fig. 4), with an average of 0.825 in. (21 mm). From analysis, shear failure occurred at a relative displacement of 0.79 in. (20 mm), as indicated in Fig. 4 by the intersection of the predicted force-deformation curve and calculated shear force capacity curve. The plastic displacements at shear failure were found by subtracting elastic displacements from the relative displacements.

The onset of shear failure resulted in the concentration of deformations in a single critical crack. All added plastic rotations from an increase in vertical displacement were no longer shared among the cracks, resulting in an unstable response and dramatic increase in crack width at the critical crack. By monitoring the crack widths during the structural test, it was clear which crack would result in catastrophic shear failure and separation of the test specimen following the onset of shear failure.

For example, as deck A's midspan plastic displacement increased from 0.76 in. to 0.89 in. (19 mm to 23 mm), the single critical crack that formed 10 in. (250 mm) from the midspan increased its width from about 0.1 in. to 0.3 in. (3 mm to 8 mm), while the other cracks closed or remained constant (Fig. 6). Figure 5 shows the failure plane at this crack and complete member separation.

Based on the formation of three cracks and assumed constant crack width through the critical region, the theory presented in this paper calculates a crack width of 0.073 in. (1.9 mm) at shear failure, which agrees well with the measured crack width at the onset of shear failure of 0.079 in. (2.0 mm). If four primary cracks are assumed, the theory gives an average crack width of 0.055 in. (1.4 mm) at failure. Differences between the average crack width from theory and measured maximum crack width are due to variations in the measured crack widths through the critical region.

The ratio of ultimate moment to cracking moment indicates the length over which cracks might develop from midspan in both directions. Taken with the crack spacing s of 5 in. (130 mm), either three or five cracks should develop. The results lay between these two possibilities. Therefore, it is of interest that in two cases three primary cracks developed and in the third case four primary cracks developed. For three cracks to develop, the length of cracking had to exceed 5 in. from the midspan (a midspan crack and two cracks 5 in. on either side of this first crack). For a fourth primary crack to develop, the length for potential cracking had to reach or exceed 10 in. (250 mm) from the midspan.

The ultimate moment is determined from the flexural expression of the ultimate tension force multiplied by the distance between the centroids of the tension and compression areas. The ultimate tension force T can be determined for the three $\frac{3}{8}$ in. (10 mm), Grade 270 (1860 MPa) prestress strands and two no. 3 (10M), Grade 60 (410 MPa) reinforcing bars placed at mid-depth of the precast concrete slab.

$$T = 3A_{ps}f_{su} + 2A_s f_y = 3(0.085)(270) + 2(0.11)(60) = 82.1 \text{ kip (365 kN)}$$

A_{ps} = area of one prestressing strand

f_{su} = ultimate stress capacity of prestressing strands

A_s = area of one reinforcing bar

f_y = yield stress of the mild steel reinforcement

The depth of the compression block is found by equating the compression force to the tension force and solving for a , resulting in a of 0.805 in. (20.4 mm). Ultimate moment capacity M_u can be determined using this value.

$$M_u = T \left(d - \frac{a}{2} \right) = 82.1 \left(5.88 - \frac{0.805}{2} \right) = 449 \text{ kip-in. (50.7 kN-m)}$$

Cracking moment M_{cr} is based on the tensile capacity of the 7 ksi (48 MPa) precast concrete (with modulus-of-rupture tensile strength f_t of 0.627 ksi [4.32 MPa]), which was determined by the American Concrete Institute's (ACI's) *Building Code Requirements for Structural Concrete (ACI 318-05) and Commentary (ACI 318R-05)*⁵ Eq. (9-10) and the amount of precompression from the prestressing strands.

$$f_t = 7.5\sqrt{f'_c} \quad \text{ACI 318-05 Eq. (9-10)}$$

$$\frac{M_{cr}c}{I} = f_t + \frac{p}{A}$$

where

I = composite moment of inertia

p = axial force from prestressing

A = cross-sectional area of precast concrete slab

Because the precast and cast-in-place concrete slabs have different design concrete strengths of 7 ksi and 5 ksi (48 MPa and 34 MPa), respectively, the composite moment of inertia I of 775 in.⁴ ($323 \times 10^6 \text{ mm}^4$) and distance from

the composite neutral axis to the extreme tension fiber c of 3.59 in. (91.2 mm) are used in the previous expression. Strand stress at the time of testing f_{ts} can be calculated.

$$f_{ts} = 0.75f_{su} - f_{sh} = 0.75(270) - 13 = 189.5 \text{ ksi (1307 MPa)}$$

At the time of stressing, the elastic shortening loss f_{sh} is 13 ksi (90 MPa). Jacking stress is 75% of the ultimate stress. The prestressing force p with three $3/8$ -in.-diameter (10 mm) strands is calculated:

$$p = 3A_{ps}f_{ts} = 3(0.085)(189.5) = 48.3 \text{ kip (215 kN)}$$

As the strands are placed at the centerline of the precast concrete slab, no bending occurs from prestressing. Thus, the cracking moment is determined.

$$M_{cr} = \frac{I}{c} \left(f_t + \frac{p}{A} \right) = \frac{775}{3.59} \left(0.627 + \frac{48.3}{78} \right) \\ = 269 \text{ kip-in. (30.4 kN-m)}$$

The ratio of cracking to ultimate moment r_{cu} is 0.599. Because of linear bending, this ratio is also the distance where cracking might develop (measured from the support) divided by half the distance between supports. Thus, the distance from the reaction point to the end of the cracking region l_{cr} can be calculated.

$$l_{cr} = \frac{l}{2} r_{cu} = \frac{62}{2} (0.599) = 18.6 \text{ in. (472 mm)}$$

The distance l_{sp} from the midspan where cracking might occur can be determined.

$$l_{sp} = \frac{l}{2} - l_{cr} = \frac{62}{2} - 18.6 = 12.4 \text{ in. (315 mm)}$$

Based on this analysis, cracking is expected to be distributed for about 12 in. (300 mm) on either side of the midspan. With a crack spacing of 5 in. (130 mm), two cracks should form on each side of the midspan, for a total of five cracks, including the midspan crack. For decks B and C, three full-width cracks developed, and for deck A, four full-width cracks developed with two on one side of the midspan and one on the other side.

The National Cooperative Highway Research Program's (NCHRP's) *Guide for Mechanistic-Empirical Design of New and Rehabilitated Pavement Structures*⁶ defines modulus of rupture f_t as

$$f_t = 9.5 \sqrt{f'_c}$$

This results in a cracking stress of 0.795 ksi (5.48 MPa). Using this NCHRP-defined cracking strength and solving for the cracking moment as done previously gives M_{cr} of 305 kip-in. (34.5 kN-m). Thus the ratio of cracking to ultimate moment is 0.680, with the distance from the support to the region of cracking of 21 in. (530 mm). In this case, the distribution of cracking from the midspan is $31 - 21 = 10$ in. (250 mm). Using the NCHRP definition for modulus of rupture and crack spacing s of 5 in. (130 mm), the total number of cracks that can form would be either three or five because the result is on the dividing line.

Five flexural cracks developed in all three composite deck slabs, but they were not all full-width (primary) cracks that were visible from the sides of the test unit. Therefore, the additional part-width cracks that were only visible on the underside of the test unit did not contribute significantly to the plastic rotations through the critical region. This was confirmed by the small width of these cracks.

The fact that deck A developed the nonsymmetric pattern of four primary cracks rather than the symmetric pattern of five cracks demonstrates that the fourth crack occurred due to a slight variation in local concrete material properties. With more than three cracks forming, this indicated that the day-of-test concrete compressive strength for deck A was weaker than for decks B and C, reducing its cracking moment and increasing the length that cracking can occur.

Deck A had a day-of-test concrete compressive strength of 6.94 ksi (47.9 MPa), while decks B and C had day-of-test concrete compressive strength of 7.35 ksi (50.7 MPa). The higher concrete strength for the precast concrete deck slabs B and C explains why only three primary cracks developed in these tests.

Using measured day-of-test concrete strengths and modulus of rupture defined by NCHRP, the length that cracking might occur from the midspan was slightly less than 10 in. (250 mm) for decks B and C and slightly larger than 10 in. for deck A. In this approach, three cracks would be expected for decks B and C and five cracks for deck A. However, using the ACI 318-05 expression for cracking strength resulted in the length from midspan that cracking might occur to be greater than 10 in. for all three decks. Therefore, five cracks for each slab would be predicted using the ACI 318.

Summary

Shear failures were observed at large displacement for all three full-scale decks tested in positive bending. The composite concrete deck consisted of a prestressed, precast concrete deck unit with a cast-in-place concrete topping slab that completed the section and provided the final riding surface on a bridge. Failures occurred along a single flexure-shear crack plane. In this study the onset of shear

failure and the degrading response after shear failure were investigated. The results demonstrate that it is possible to determine the force and displacement at shear failure by finding the intersection of the force-deformation curve from flexural analysis¹ and the degrading shear strength–deformation curve from the modified compression field theory, as well as geometric considerations of the structure.

For these deck slabs, the initial shear strength was greater than the demand. This allowed the majority of the behavior to be determined from flexural analysis. However, the shear strength decreased quickly as a function of crack width and related vertical displacement, and the final failure at large deformation was from shear. This final failure mode occurred at displacements that will not be seen in the field from service load or from extreme earthquake loading.

This study demonstrated that the measured slow decline in force with increased displacement following peak force for two of the deck slabs was due to the onset of shear failure. This was not clear at the time of the tests or when writing the first paper¹ on these tests. By comparing theoretical and measured crack widths, the onset of shear failure is clearly defined as an unstable crack-width growth at one of the flexure-shear cracks with a simultaneous reduction in width at the other cracks. In all three cases, crack widening occurred at the critical flexure-shear crack immediately following peak force and the onset of shear failure.

Conclusion

Final conclusions can be summarized as follows:

- Precast concrete deck panels with cast-in-place topping slab act compositely to failure regardless of the level of deck-panel roughening and with no reinforcement crossing the interface between slabs.
- The final failure mode at wide-open, diagonal flexure-shear cracks occurred at vertical displacements that are far beyond expected displacement demands from service loads and from severe seismic shaking.
- The modified compression field theory can be used to accurately determine the force and vertical displacement at the onset of diagonal shear failure that results in complete separation.

References

1. Dowell, R. K., and J. Smith. 2006. Structural Tests of Precast Concrete Deck Panels for California Freeway Bridges. *PCI Journal*, V. 51, No. 2 (March–April): pp. 76–87.
2. Dowell, R. K. 2005. Structural Tests of Precast Deck Panels for the 22 Freeway. Structural engineering

research project report no. SERP-2005/1, San Diego State University, San Diego, CA.

3. Post, Buckley, Schuh & Jernigan. 2005. SR-22 HOV Widen Design Build Precast/Prestressed Concrete Composite Deck Panels, Test Procedures and Performance Criteria. Report for Granite-Myers-Rados, joint venture, PBS&J, San Diego, CA.
4. Collins, M. P., and D. Mitchell. 1997. *Prestressed Concrete Structures*. Toronto, ON, Canada: Response Publications.
5. American Concrete Institute (ACI) Committee 318. 2005. *Building Code Requirements for Structural Concrete (ACI 318-05) and Commentary (ACI 318R-05)*. Farmington Hills, MI: ACI.
6. NCHRP. 2004. *Guide for Mechanistic-Empirical Design of New and Rehabilitated Pavement Structures*. Final report, NCHRP project 1-37A. Washington, DC: Transportation Research Board, National Research Council.

Notation

- a = depth of compression block
- A = cross-sectional area of precast concrete slab
- A_{ps} = area of one prestressing strand
- A_s = area of one reinforcing bar
- b = slab width
- c = distance from the composite neutral axis to the extreme tension fiber
- d = distance from the extreme compression fiber to centroid of primary tension reinforcement
- f'_c = unconfined concrete strength
- f_{sh} = elastic shortening loss
- f_{su} = ultimate stress capacity of prestressing strands
- f_t = modulus-of-rupture tensile strength
- f_{ts} = strand stress at time of stressing
- f_y = yield stress of mild steel reinforcement
- I = composite moment of inertia
- j = constant multiplied by d to get the distance between

tension and compression centroids

k = crack length along incline

l = span length between supports

l_{cr} = distance from the reaction point to the end of the cracking region

l_{sp} = distance from midspan where cracking might occur

M_{cr} = cracking moment

M_u = ultimate moment capacity

n = number of primary cracks

p = axial force from prestressing

P = applied load

q = maximum aggregate size

r_{cu} = the ratio of cracking to ultimate moment

R = reaction force

s = crack spacing

T = ultimate tension force capacity

v_{ci} = concrete shear stress capacity

V_c = vertical concrete shear force capacity

V_{ci} = concrete shear force capacity along incline

w = crack width

Δ_p = midspan plastic displacement

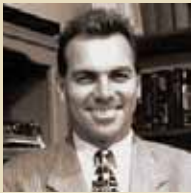
θ = angle of crack plane from the horizontal

θ_{cr} = amount of plastic rotation attributed to a single crack

θ_p = total plastic rotation at the critical section

θ_{pe} = rotation at the end of the span from plastic deformations

About the authors



Robert K. Dowell, PhD, P.E., is a structural engineering professor in the Department of Civil, Construction and Environmental Engineering at San Diego State University in San Diego, Calif.



Roy Auer, P.E., is a bridge engineer for the California Department of Transportation in San Diego, Calif.

Synopsis

Full-scale precast concrete deck slabs designed for bridge structures were tested to failure under simple bending with varying levels of roughness between the precast concrete slab and cast-in-place concrete topping slab. Because no horizontal shear slip occurred between the precast and cast-in-place concrete slabs, the behaviors were nominally the same for the three tests loaded in positive bending. In an earlier paper, Dowell compared the measured and predicted force-deformation results, which had good agreement, until the onset of failure, with nonlinear prediction analyses based on flexural response only. Not considered before the tests, as reflected in the prediction analyses reported in the earlier published study, was the flexure-shear mode of failure observed for all three tests.

The structural tests demonstrated that the precast and cast-in-place concrete slabs acted compositely to large displacements, with the final failure plane occurring through both slabs as if they were one, at a single,

wide-open, inclined flexure-shear crack. Because the purpose of the structural tests and analyses was to demonstrate that precast and cast-in-place concrete topping slabs act compositely under working loads, a complete understanding of the failure mechanism was of secondary importance to the project because this occurred at displacements well beyond the desired performance. It is of interest now, however, to revisit the data and observed behaviors from the structural tests to give a more complete picture of the failures, especially because critical crack widths were measured throughout the tests but were not previously published.

In this paper, the measured and observed shear failures for all three composite slabs tested in positive bending are compared to analytically determined force and displacement values at failure. This is found using the modified compression field theory and geometry considerations of a simple beam with well-defined and idealized flexure-shear cracks. Theoretical and measured crack widths and plastic hinge rotations at midspan are also compared in the paper.

Keywords

Composite section, crack width, flexure-shear failure, plastic rotation, slab.

Review policy

This paper was reviewed in accordance with the Precast/Prestressed Concrete Institute's peer-review process.

Reader comments

Please address any reader comments to journal@pci.org or Precast/Prestressed Concrete Institute, c/o *PCI Journal*, 200 W. Adams St., Suite 2100, Chicago, IL 60606. 